Experimental evidence on the origin of Ca-rich carbonated melts formed by interaction between sedimentary limestones and mantle-derived ultrabasic magmas

Article *in* Geology · October 2021

DOI: 10.1130/G49621.1

6 authors, including:

Michele Lustrino
Sapienza University of Rome
147 PUBLICATIONS **4,861** CITATIONS
SEE PROFILE

Natascia Luciani
Vrije Universiteit Amsterdam
14 PUBLICATIONS **50** CITATIONS
SEE PROFILE

Vincenzo Stagno
Sapienza University of Rome
90 PUBLICATIONS **1,501** CITATIONS
SEE PROFILE

Piergiorgio Scarlato
National Institute of Geophysics and Volcanology
284 PUBLICATIONS **5,477** CITATIONS
SEE PROFILE

Accepted for publication in:

GEOLOGY

Experimental evidence on the origin of Ca-rich carbonated melts formed by interaction between sedimentary limestones and mantle-derived ultrabasic magmas

Michele Lustrino[1,2]*, Natascia Luciani[1,3], Vincenzo Stagno[1,5], Silvia Narzisi[1], Matteo Masotta[4], Piergiorgio Scarlato[5]

1 Dipartimento di Scienze della Terra, Sapienza Università di Roma, P.le A. Moro, 5, 00185 Roma, Italy

2 CNR – Istituto di Geologia Ambientale e Geoingegneria (IGAG), c/o Dipartimento di Scienze della Terra, Sapienza Università di Roma, P.le A. Moro, 5, 00185 Roma, Italy

3 Faculty of Science, Vrije Universiteit Amsterdam, De Boelelaan 1085, 1081 HV Amsterdam, the Netherlands

4 Dipartimento di Scienze della Terra, Università degli Studi di Pisa, Via S. Maria, 53, 56126, Pisa, Italy

5 Istituto Nazionale di Geofisica e Vulcanologia, Sezione di Roma1, Via di Vigna Murata, 605, 00143, Roma, Italy

* Corresponding author. email: michele.lustrino@uniroma1.it

ABSTRACT

Three strongly to moderately SiO_2-undersaturated volcanic rocks from the Bohemian Massif have been mixed with 10, 30 and 50 wt% $CaCO_3$ and melted at 1100, 1200 and 1300 °C at 2 kbar to evaluate the maximum amount of carbonate that can be assimilated by natural ultrabasic melts at shallow depths. Experiments reveal a surprisingly complete dissolution of the $CaCO_3$, only rarely reaching carbonate saturation, with typical liquidus phases represented by olivine, spinel, melilite and clinopyroxene. Only in the runs with the most SiO_2-undersaturated compositions, abundant monticellite forms instead of clinopyroxene. For all starting mixtures, strongly ultrabasic (SiO_2 down to 15.6 wt%), lime-rich (CaO up to 43.6 wt%), ultracalcic (CaO/Al_2O_3 up to ~27) melt compositions are produced at 1200 and 1300 °C, with up to ~25 wt% dissolved CO_2. When present,

quenched olivine shows much higher forsterite content (Fo_{95-97}) than olivine in the natural samples (Fo_{79-85}).

The two major results of this study are: 1) silicate-carbonatite melt compositions do not necessarily imply the existence of carbonatitic components in the mantle, being them produced also during limestone assimilation, and 2) Fo-rich olivines cannot be used to infer any primitive character of the melt nor high potential temperature (Tp).

INTRODUCTION

Near-solidus partial melting of a carbonated mantle produces carbonatitic liquids (e.g., Hammouda and Keshav, 2015). An increase of the melting degree results in a more diluted carbonate component, due to the increasing contribution of the partial melts derived from the silicate matrix. As a result, melts with a broad spectrum of compositions can be produced, varying from nearly pure carbonatitic (i.e., without SiO_2) to basaltic (Gudfinnsson and Presnall, 2005; Green, 2015; Yaxley et al., 2019; Weidendorfer et al., 2020; Keshav and Gudfinnsson, 2021).

A secondary, but frequently overlooked mechanism for the origin of carbonatitic magmas has little relations with upper mantle dynamics. Indeed, carbonatite melts can be produced at crustal depths via sedimentary carbonate anatexis caused by hydrothermal fluids with high $H_2O/(H_2O+CO_2)$ (~0.95; Lentz, 1999) released by deep-seated solidifying magmas. The interaction between carbonatite (both mantle- and crustal-derived) and silicate components leads to the formation of a group of poorly-characterized compositions, classified as silicocarbonatites (Le Maitre, 2002). Hybrid compositions can result after the assimilation of sedimentary carbonates by ultrabasic melts (e.g., Lustrino et al., 2019, 2020; Sklyarov et al., 2021) or, vice versa, of crustal silicate rocks by carbonatitic to ultrabasic-ultracalcic CO_2-bearing melts (e.g., Ackerman et al., 2021). In this experimental study, we document the formation of silicate-carbonatite melts through the interaction between basaltic s.l. melts with limestones and dolostones. Large amounts of CO_2 can be dissolved at crustal depths, and then abruptly released through simple upwelling, cooling and crystallization magma mechanisms.

MATERIALS AND METHODS

Three compositionally distinct volcanic rocks from the Bohemian Massif were used as starting material for carbonate-melt interaction experiments (Table 1): 1) a Paleocene melilite-olivine-nephelinite (polzenite, sampled on the Great Devil's Wall, Osečná Complex, Czech Republic) with

~38.5 wt% SiO_2 (sample BM1), 2) a Paleocene monticellite-bearing melilitite (vesecite, at the type locality Vesec village, Czech Republic) with ~30.3 wt% SiO_2 (sample BM2), and 3) an olivine basanite (collected at the village of Jauernick, near the town of Görlitz, Germany) with ~43 wt% SiO_2 (sample BM3). The composition of the three volcanic rocks resemble mafic melts in equilibrium with a peridotitic assemblage, being characterized by high contents of MgO (15.9-17.1 wt%), Ni (300-440 ppm) and Cr (710-1010 ppm), and with Mg# ~74 (assuming $Fe^{3+}/\Sigma Fe = 0.15$).

Each starting material was subject to two cycles of melting at 1400 and 1450 °C for up to 12 hours, quenching as glass and powdering, and then mixed with 10, 30 and 50 wt% of reagent grade $CaCO_3$ and inserted in Pt capsules. A total of forty-one isobaric experiments was performed at 2 kbar in a non-end loaded piston cylinder, using standard 1" low pressure assemblies (Masotta et al., 2012). The pressure of 2 kbar was selected to mimic the interaction between silicate melts and the base of the overthickened limestone thrusts of central Apennines, located at depth of ~5-6 km (Barchi et al., 2003). Mixtures were maintained at temperatures of 1100, 1200 and 1300 °C for 1 to 12 hours and then quenched (Table 1). Full details on the analytical techniques and bulk analyses of natural rocks and experimental compositions (including mineral compositions) are reported in the Data Repository.

RESULTS

Vesicles are common in all the experimental runs, thereby indicating the attainment of CO_2 saturation in all the residual melts. Runs carried out at 1100 °C are either sub-solidus or are characterized by compositionally heterogeneous glass pools. Runs carried out at 1200 and 1300 °C are characterized by large patches of homogenous glass containing scarce quench crystals and, for this reason, have been used to constrain the composition of the hybrid melts. The most important compositional changes of experiments are presented below and are ordered according to the increasing SiO_2 content of the starting material.

BM2 experiments. Only the experiment doped with 50 wt% of $CaCO_3$ at 1300 °C is supra-liquidus (except for minor amount of quench crystals of calcite). All the other experiments crystallized Ca-rich (CaO ~2.0-2.5 wt%) and Mg-rich olivine (Fo_{96-97}) always associated with minor monticellite (La_{35-47}; Mg# = 84-94) and Al-Fe-Mg spinel (occasionally chromite-rich) ± melilite. No substantial chemical differences among the glasses quenched at 1200 and 1300 °C experiments can be observed (Fig. 1). The experiments performed at 1300 °C show a negative correlation between all the major oxides of the melt and $CaCO_3$ added, with very high coefficients of

determination [R^2 varying from 0.94 (FeO_{tot}) to 1.00 (Al_2O_3)]. The amount of CaO in the residual melt and the estimated CO_2 content (i.e., 100 – glass wt% total from microprobe analyses), show a positive correlation with the amount of $CaCO_3$ added (R^2 = 0.99 for both oxides). The SiO_2 content ranges from ~30 wt% to ~16 wt%, while CaO increases from ~23 wt% to ~44 wt% with increasing $CaCO_3$ added.

BM1 experiments. Runs at 1100 °C do not crystallize olivine, but abundant kushiroite-rich (Al_2O_3 = 9.4-10.6 wt%) clinopyroxene, melilite and spinels, also with calcite ± perovskite. Olivine (Fo_{95-97}; CaO = 1.1-2.8 wt%), Al-rich clinopyroxene (Al_2O_3 = 7.7-10.6 wt%) and spinel are present in all the experiments at 1200 and 1300 °C, with calcite found only in experiments doped with 30 wt% and 50% $CaCO_3$. Also in this case, the 1200 and 1300 °C runs produced residual melts with nearly indistinguishable compositions (Fig. 1). Major oxides show negative correlations with the amount of $CaCO_3$ added, with R^2 mostly clustering around 0.94-0.99. Experiments carried out at 1200 °C show lower R^2 with $CaCO_3$, likely due to sub-liquidus conditions and the selective removal of specific oxides by nearby quenched minerals (e.g., see the drop of MgO in charges doped with 10 wt% $CaCO_3$, likely related to strong MgO incorporation in olivine). As the amount of $CaCO_3$ increases, the concentration of SiO_2 in the residual melt decreases from ~40.0 wt% to ~29.8 wt%. At the same time, while CaO of the residual melt increases from ~13.4 wt% to 30.5 wt%, coupled with an increase of CO_2 from ~1 to ~9 wt%.

BM3 experiments. Residual melts obtained at 1200 and 1300 °C show similar major oxide compositions, defining again a nearly perfect negative correlation with the amount of $CaCO_3$ added to the starting material (R^2 = 0.96-1.00). As reported above, the concentration of CaO in the melt is also perfectly correlated with the amount of $CaCO_3$ added (R^2 = 1.00). However, the estimated amount of CO_2 is less correlated with $CaCO_3$ (R^2 = 0.76), perhaps due to CO_2 lost in the abundant vesicles. The oxides of BM3 and BM1 glasses show a nearly complete overlap, except for TiO_2, which is more abundant in the BM3 starting composition. The modal content of olivine (Fo_{94-97}) tends to decrease with $CaCO_3$ increasing, due to the enlargement of clinopyroxene and melilite stability fields.

Discussion

Maximum amount of carbonate digestion by a natural melt

CaO- and MgO-rich ultracalcic and ultrabasic compositions are interpreted in literature as the result of low-degree partial melting of carbonated peridotite sources (e.g., Hammouda and

Keshav, 2015; Lustrino et al., 2021). However, experimental melts from this study document that such kind of ultracalcic and ultrabasic compositions can be easily obtained by magma-carbonate interaction at crustal depths. In particular, while previous studies focused on the assimilation of carbonate material by basaltic (Iacono Marziano et al., 2008; Mollo et al., 2010; Carter and Dasgupta, 2015; Di Stefano et al., 2018) to andesitic-dacitic melts (Carter and Dasgupta, 2016), our experiments were carried out on natural ultrabasic and strongly silica-undersaturated melts.

Fig. 1 shows the increase of CaO and CO_2, as well as the decrease of SiO_2 content in the melt as function of the amount of $CaCO_3$, showing a good agreement with literature data on similar experiments. Literature compositions reach carbonate saturation at contents of <20 wt% of $CaCO_3$ added, proved by the presence of quenched calcite crystals in the experimental runs (Mollo et al., 2010; Jolis et al., 2013). Carter and Dasgupta (2015) report the presence of variable amounts of quenched glass (~9 to ~69 vol%) associated with abundant calcite (~26 to ~50 vol%) and other minerals (i.e., clinopyroxene, plagioclase, spinel and scapolite, in order of lower abundance). This phase assemblage testifies to a prolonged calcite saturation for a 1:1 mixture of a synthetic basalt and $CaCO_3$ equilibrated at 1100-1200 °C and 5-10 kbar. In contrast, our results only rarely reach carbonate saturation, as evidenced by the presence of minute amounts (<5 vol% of the capsule) of calcite microlites.

Experiments from literature are characterized by higher degrees of crystallization of Ca-Mg-Al-Fe-rich clinopyroxene (e.g., Iacono-Marziano et al., 2008; Mollo et al., 2010) during carbonate assimilation. This leads to the formation of residual melts depleted in SiO_2 and enriched in alkalis. These chemical variations are not observed in our experiments, where only CaO and the estimated CO_2 increase in the residual melt as the added $CaCO_3$ increases.

Changes in olivine crystal chemistry

The key chemical features of olivine crystallized from $CaCO_3$-doped melts are summarized in Fig. 2, where the maximum CaO and the maximum Fo contents of olivine are plotted as function of $CaCO_3$ added to the experimental charge. The maximum CaO content in olivine is 2.84 wt%, 2.21 wt% and 2.46 wt% for BM2 (vesecite), BM1 (polzenite), and BM3 (basanite), respectively (Fig. 2a). Our results show an increase in CaO content in olivine only for BM1 and BM3 compositions (Fig. 2a), whereas the forsterite content remains more or less unchanged in all the experiments (Fig. 2b) with increasing $CaCO_3$ addition. This is partially contrasting, compared to what reported in previous works (Iacono Marziano et al., 2008; Mollo et al., 2010; Di Stefano et al., 2018).

Overall, the increasing solubility of CaO in the melt favours Ca incorporation in the M2 site of olivine, thereby increasing the Ca → Fe^{2+} substitutions (Di Stefano et al., 2018). On the other hand, Mg in the M1 site of olivine increases with increasing $CaCO_3$ assimilation due to the fact that Ca cations are incorporated in the M2 site only. The resulting effect is an increase of the Fo content in olivine, as already experimentally noted (Jolis et al., 2013; Di Stefano et al., 2018) and found in natural systems (e.g., Lustrino et al., 2019). The constant high forsterite content of the quenched olivines indicates a sort of saturation of Ca-Fe-Mg ions in the M1 and M2 sites. The value of $KD(Fe-Mg)^{olivine/melt}$ calculated to equilibrate Fo_{96} olivine in equilibrium with a Mg# = 74 melt (~0.12) is much lower than the expected equilibrium range between olivine and basaltic melts (0.27-0.39; see discussion in Lustrino et al., 2021). As consequence, high-Fo olivine crystals can be no longer considered as an indicator for the primitive magma compositions nor for the elevated potential temperature (Tp) of crystallizing magmatic systems.

Conclusions

The effects of addition of 10, 30 and 50 wt% $CaCO_3$ on three different natural SiO_2-undersaturated compositions was investigated at 2 kbar and 1100, 1200 and 1300 °C. We demonstrate that, upon availability of the energy required for the assimilation of crustal material (i.e., heating of crustal rocks to melting temperature and latent heat of fusion), up to 50 wt% of $CaCO_3$ can be assimilated by strongly SiO_2-ultrabasic liquids, producing strongly SiO_2-ultrabasic (SiO_2 down to 15.6 wt%) ultracalcic melts (CaO/Al_2O_3 = 1.6-26.9). The major oxide content of these melts varies as a function of the dilution by the CaO and CO_2 components and eventual mineral saturation. The resulting ultracalcic melts are extremely poor in SiO_2, (maximum CIPW normative larnite = 19.3 wt%), rich in MgO (average 11.9 ± 2.0 wt%), and with an Mg# (71-84) proportional to the amount of $CaCO_3$ assimilated. These compositional changes are particularly relevant to interpret the genesis of some ultrabasic compositions cropping out in central Italy (e.g., Polino, San Venanzo, Cupaello volcanoes; Lustrino et al., 2011), albeit the implications can be exported in all the igneous crustal settings where mafic magmas are in contact with thick carbonate systems.

The main conclusions raised by this experimental study are: 1) ultrabasic magmas can assimilate limestone up to a 1:1 ratio reaching only minimum amount of calcite saturation; 2) olivine is the liquidus phase in $CaCO_3$-doped strongly ultrabasic magmas, replaced or joined by clinopyroxene and melilite in $CaCO_3$-doped mildly ultrabasic magmas; 3) monticellite rims develop around Ca-rich olivine crystals when strongly SiO_2-undersaturated melts assimilate carbonate (as for example

recorded at Polino volcano; Lustrino et al., 2019); 4) olivine crystallizing from $CaCO_3$-doped ultrabasic magmas are characterized by strongly forsteritic compositions (up to Fo_{97}), a feature that shares more similarities with skarn than with alleged primitive magma compositions generated at high Tp; 5) the $KD(Fe\text{-}Mg)^{olivine/melt}$ for CaO-rich ultracalcic ultrabasic compositions (>0.4-0.5; Dalton and Wood, 1993; Lustrino et al., 2021) is higher than that observed for natural basaltic systems (~0.3; Roeder and Emslie, 1970); 6) the maximum inferred CO_2 content in the $CaCO_3$-doped melt reaches ~25 wt%, a feature that can have strong impact on the eruptive styles of natural systems, because it can abruptly exsolve with magma approaching to the surface, giving rise to violent paroxysms; 7) the presence of CaO- and CO_2-rich magmas, as well as primary carbonate crystallization or the presence of immiscible carbonate-silicate droplets and the presence itself of carbonatitic magma are features not necessarily related to the presence of carbonated mantle.

Acknowledgements

Warmest regards to M. Serracino and M. Albano (IGAG-CNR) for the assistance during EMP and SEM work. Thanks to Silvio Mollo (Rome) for his availability to discuss basic concepts of magma-limestone assimilation. PRIN 2017 Project 20177BX42Z_005 and Ateneo La Sapienza grants (2019–2020) are deeply acknowledged. ML thanks Jörg Büchner for providing the BM3 sample, the organizers of the excellent Conference Basalt 2013 at the Senckenberg Museum of Natural History Görlitz (Germany), for the great excursion during which ML collected the samples, Vladislav Rapprich and Ondřej Pour (Prague) for providing olivine EMP analyses of Great Devil's wall (BM1 sample) and Mike Stern for his little shoes.

Figure 1: CaO (a), CO_2 (b) and SiO_2 (c) in the experimental glasses obtained at 1200 and 1300 °C vs. $CaCO_3$ added. Literature experiments mixing $CaCO_3$ with natural and synthetic basaltic compositions are reported for comparison. Light grey triangle: 1200 °C, 5 kb + 1 wt% H_2O; (Mollo et al., 2010); light grey circle: 1300 °C, 5 kb + 1 wt% H_2O (Mollo et al., 2010); grey square: 1150 °C, 1 atm (Iacono Marziano et al., 2008); tilted grey square: 1050 °C, 2 kb + 2 wt% H_2O (Iacono Marziano et al., 2008); light brown square: 1100 °C, 5 kb + 4 wt% H_2O (Carter and Dasgupta, 2015); yellow triangle: 1200 °C, 5 kb + 2 wt% H_2O (Jolis et al., 2013); lilac square: 1200 °C, 5 kb + 2 wt% H_2O (Deegan et al., 2010); pink tilted square: 1250 °C, 1 atm (Di Stefano et al., 2018).

Figure 2: $CaO_{olivine}$ (wt%) (a) and $Fo_{olivine}$ (b) vs. $CaCO_3$ added (wt%) in the experimental melts obtained adding variable amounts of $CaCO_3$. Grey tilted squares and triangles: Mollo et al. (2010) at 1150 °C and 1 wt% H_2O and 1200 °C and 1 wt% H_2O, respectively. Orange tilted squares and triangles indicate the experiments of Di Stefano et al. (2018) at 1250 and 1150 °C at 1 atm. Pink circles indicate the experiments of Iacono Marziano et al. (2008) at 1150 °C at 2.1 kb with the addition of 1 wt% H_2O. The olivine compositions of the starting samples (BM1, BM2 and BM3) are reported for comparison.

Table 1: Natural samples and quenched glasses used for experiments. Mg# = 100 x $Mg/(Mg+Fe^{2+})$ assuming $Fe^{3+}/\Sigma Fe = 0.15$.

References

Ackerman, L., Rapprich, V., Polak, L., Magna, T., Mclemore, V. T., Pour, O., and Cejkova, B., 2021, Petrogenesis of silica-rich carbonatites from continental rift settings: a missing link between carbonatites and carbonated silicate melts?: Journal of Geosciences, v. 66, p. 71-87.

Barchi, M., Minelli, G., Magnani, B., Mazzotti, A., 2003, Line CROP 03: Northern Apennines: Memorie Descrittive della Carta Geologica d'Italia, 62, 127-136.

Carter, L. B., and Dasgupta, R., 2015, Hydrous basalt–limestone interaction at crustal conditions: Implications for generation of ultracalcic melts and outflux of CO_2 at volcanic arcs: Earth and Planetary Science Letters, v. 427, p. 202-214, doi:10.1016/j.epsl.2015.06.053.

Carter, L. B., and Dasgupta, R., 2016, Effect of melt composition on crustal carbonate assimilation: Implications for the transition from calcite consumption to skarnification and associated CO_2 degassing: Geochemistry Geophysics Geosystems, v. 17, p. 3893-3916, doi: 0.1002/2016GC006444.

Deegan, F. M., Troll, V. R., Freda, C., Misiti, V., Chadwick, J. P., McLeod, C. L., and Davidson, J. P., 2010, Magma–carbonate interaction processes and associated CO_2 release at Merapi Volcano, Indonesia: insights from experimental petrology: Journal of Petrology, v. 51, p. 1027-1051, doi: 10.1093/petrology/egq010.

Di Stefano, F., Mollo, S., Scarlato, P., Nazzari, M., Bachmann, O., and Caruso, M., 2018, Olivine compositional changes in primitive magmatic skarn environments: A reassessment of divalent cation partitioning models to quantify the effect of carbonate assimilation: Lithos, v. 316, p. 104-121, doi: 10.1016/j.lithos.2018.07.008.

Green, D. H., 2015, Experimental petrology of peridotites, including effects of water and carbon on melting in the Earth's upper mantle: Physics and Chemistry of Minerals, v. 42, p. 95-122, doi: 10.1007/s00269-014-0729-2

Gudfinnsson, G. H., and Presnall, D. C., 2005, Continuous gradations among primary carbonatitic, kimberlitic, melilititic, basaltic, picritic, and komatiitic melts in equilibrium with garnet lherzolite at 3–8 GPa: Journal of Petrology, v. 46, p. 1645-1659, doi: 10.1093/petrology/egi029.

Hammouda, T., and Keshav, S., 2015, Melting in the mantle in the presence of carbon: Review of experiments and discussion on the origin of carbonatites: Chemical Geology, v. 418, p. 171-188, doi: 10.1016/j.chemgeo.2015.05.018.

Marziano, G. I., Gaillard, F., and Pichavant, M., 2008, Limestone assimilation by basaltic magmas: an experimental re-assessment and application to Italian volcanoes: Contributions to Mineralogy and Petrology, v. 155, p. 719-738, doi: 10.1007/s00410-007-0267-8.

Jolis, E. M., Freda, C., Troll, V. R., Deegan, F. M., Blythe, L. S., McLeod, C. L., and Davidson, J. P., 2013, Experimental simulation of magma–carbonate interaction beneath Mt. Vesuvius, Italy: Contributions to Mineralogy and Petrology, v. 166, p. 1335-1353, doi: 10.1007/s00410-013-0931-0.

Keshav, S., and Gudfinnsson, G. H., 2021, A reappraisal of peridotite solidus phase equilibria from 6 to 14 GPa in the system CaO-MgO-Al_2O_3-SiO_2: Journal of Petrology, v. 62, p. 1-19, doi: 10.1093/petrology/egab009.

Le Maitre, R. W. (Ed.), 2002, Igneous rocks a classification and glossary of terms, 2nd edition. Cambridge University Press, 236 pp.

Lentz, D. R., 1999, Carbonatite genesis: a reexamination of the role of intrusion-related pneumatolytic skarn processes in limestone melting: Geology, v. 27, p. 335-338, doi: 10.1130/0091-7613(1999)027<0335:CGAROT>2.3.CO;2.

Lustrino, M., Duggen, S., Rosenberg, C. L., 2011, The Central-Western Mediterranean: Anomalous igneous activity in an anomalous collisional setting: Earth-Science Reviews, v. 104, p. 1-40, doi:10.1016/j.earscirev.2010.08.002.

Lustrino, M., Luciani, N., and Stagno, V., 2019, Fuzzy petrology in the origin of carbonatitic/pseudocarbonatitic Ca-rich ultrabasic magma at Polino (central Italy): Scientific Reports, v. 9, p. 1-14, doi: 10.1038/s41598-019-45471-x.

Lustrino, M., Ronca, S., Caracausi, A., Bordenca, C. V., Agostini, S., and Faraone, D. B., 2020, Strongly SiO_2-undersaturated, CaO-rich kamafugitic Pleistocene magmatism in Central Italy (San

Venanzo volcanic complex) and the role of shallow depth limestone assimilation: Earth-Science Reviews, v. 208, p. 103256, doi: 10.1016/j.earscirev.2020.103256.

Lustrino, M., Salari, G., Rahimzadeh, B., Fedele, L., Masoudi, F., and Agostini, S., 2021, Quaternary melanephelinites and melilitites from Nowbaran (NW Urumieh-Dokhtar Magmatic Arc, Iran): origin of ultrabasic-ultracalcic melts in a post-collisional setting: Journal of Petrology, v. 62, p. 1-31, egab058, doi: 10.1093/petrology/egab058.

Masotta, M., Freda, C., Paul, T. A., Moore, G. M., Gaeta, M., Scarlato, P., and Troll, V. R., 2012, Low pressure experiments in piston cylinder apparatus: Calibration of newly designed 25 mm furnace assemblies to P = 150 MPa: Chemical Geology, v. 312, p. 74-79, doi: 10.1016/j.chemgeo.2012.04.011.

Mitchell, R. H., 2005, Carbonatites and carbonatites and carbonatites: The Canadian Mineralogist, v. 43, p. 2049-2068, doi: 10.2113/gscanmin.43.6.2049.

Mollo, S., Gaeta, M., Freda, C., Di Rocco, T., Misiti, V., and Scarlato, P., 2010, Carbonate assimilation in magmas: a reappraisal based on experimental petrology: Lithos, v. 114, p. 503-514, doi: 10.1016/j.lithos.2009.10.013.

Sklyarov, E. V., Lavrenchuk, A. V., Doroshkevich, A. G., Starikova, A. E., Kanakin, S. V., 2021, Pyroxenite as product of mafic-carbonate melt interaction (Tazheran Massif, West Baikal Area, Russia): Minerals, v. 11, 654, doi.org/10.3390/min11060654.

Weidendorfer, D., Manning, C. E., and Schmidt, M. W., 2020, Carbonate melts in the hydrous upper mantle: Contributions to Mineralogy and Petrology, v. 175, p. 1-17, doi: 10.1007/s00410-020-01708-x.

Yaxley, G. M., Ghosh, S., Kiseeva, E. S., Mallik, A., Spandler, C., Thomson, A. R., and Walter, M. J., 2019, CO_2-rich melts in Earth. In: B.N. Orcutt, I. Daniel, R. Dasgupta (Eds.), Deep carbon Past to present, pp. 129-162, doi: 10.1017/9781108677950.006.

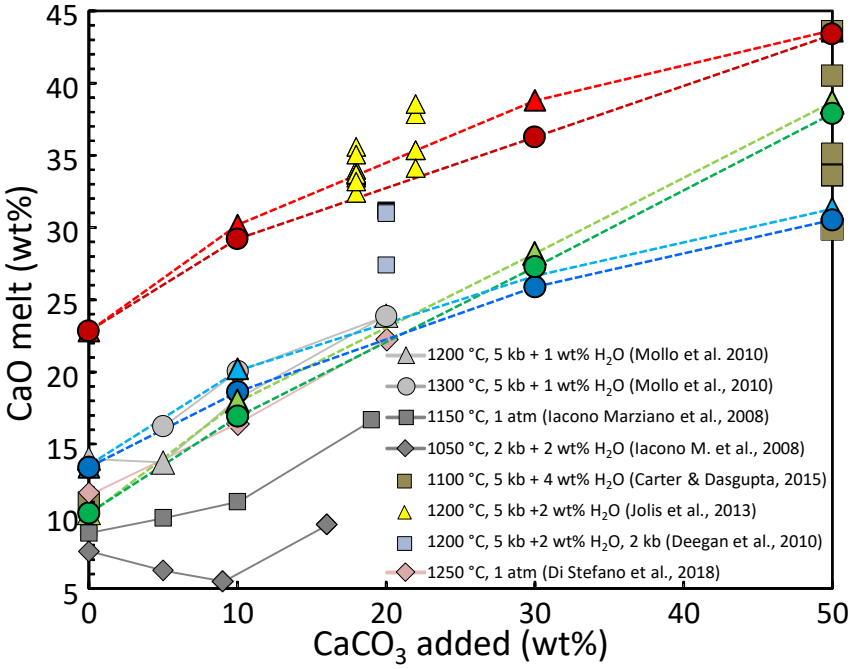
CaO melt (wt%)
CaCO3 added (wt%)
1200 °C, 5 kb + 1 wt% H2O (Mollo et al. 2010)
1300 °C, 5 kb + 1 wt% H2O (Mollo et al., 2010)
1150 °C, 1 atm (Iacono Marziano et al., 2008)
1050 °C, 2 kb + 2 wt% H2O (Iacono M. et al., 2008)
1100 °C, 5 kb + 4 wt% H2O (Carter & Dasgupta, 2015)
1200 °C, 5 kb +2 wt% H2O (Jolis et al., 2013)
1200 °C, 5 kb +2 wt% H2O, 2 kb (Deegan et al., 2010)
1250 °C, 1 atm (Di Stefano et al., 2018)

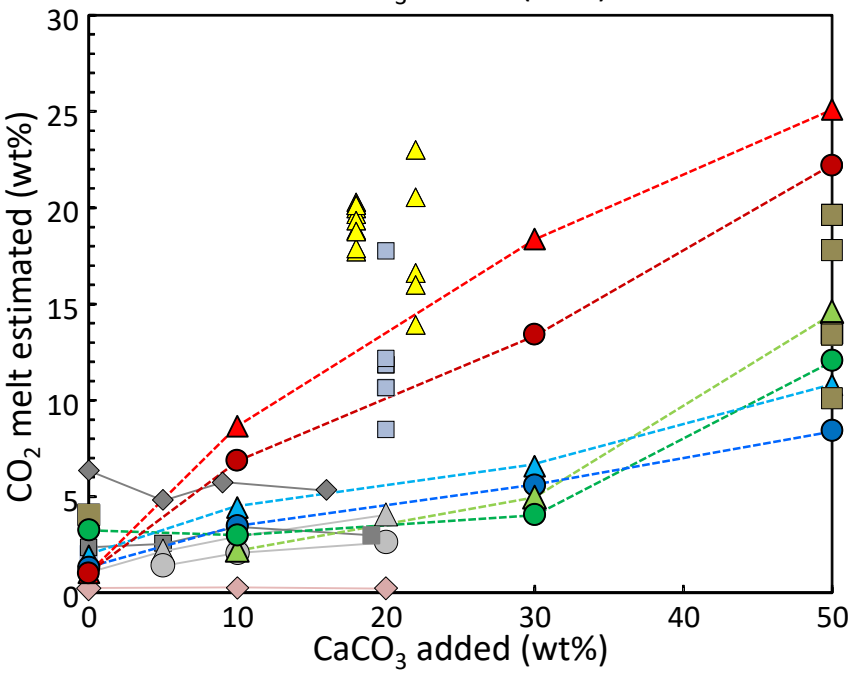
CO2 melt estimated (wt%)
CaCO3 added (wt%)

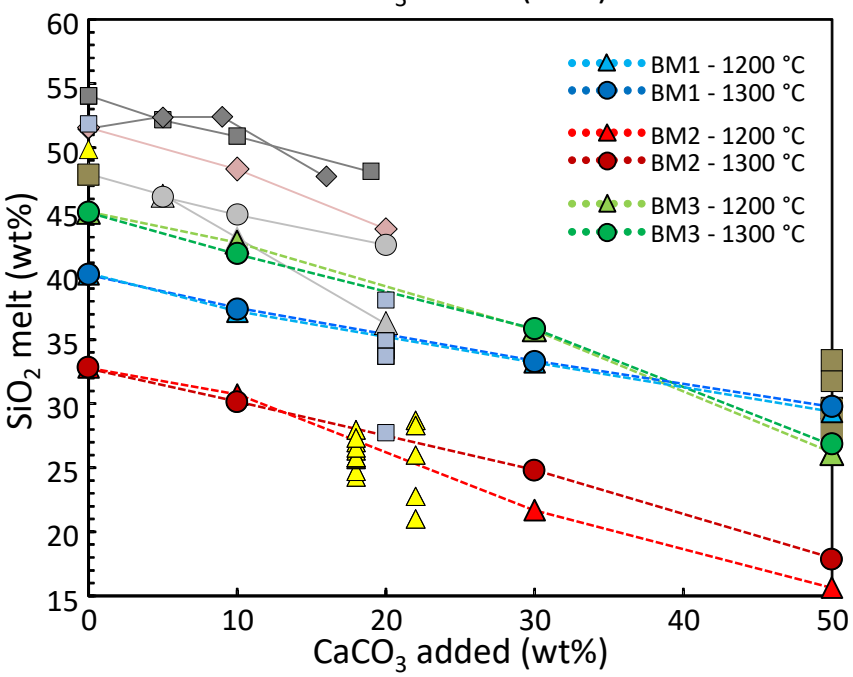
SiO2 melt (wt%)
CaCO3 added (wt%)
BM1 - 1200 °C
BM1 - 1300 °C
BM2 - 1200 °C
BM2 - 1300 °C
BM3 - 1200 °C
BM3 - 1300 °C

Fig. 1

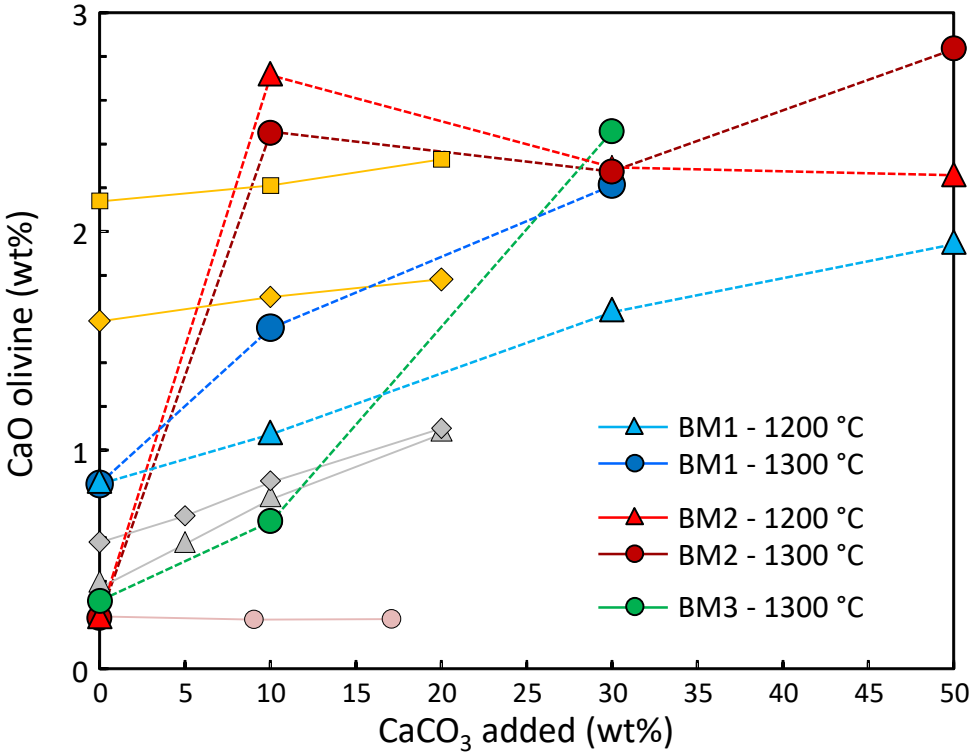
CaO olivine (wt%)
CaCO3 added (wt%)
BM1 - 1200 °C
BM1 - 1300 °C
BM2 - 1200 °C
BM2 - 1300 °C
BM3 - 1300 °C

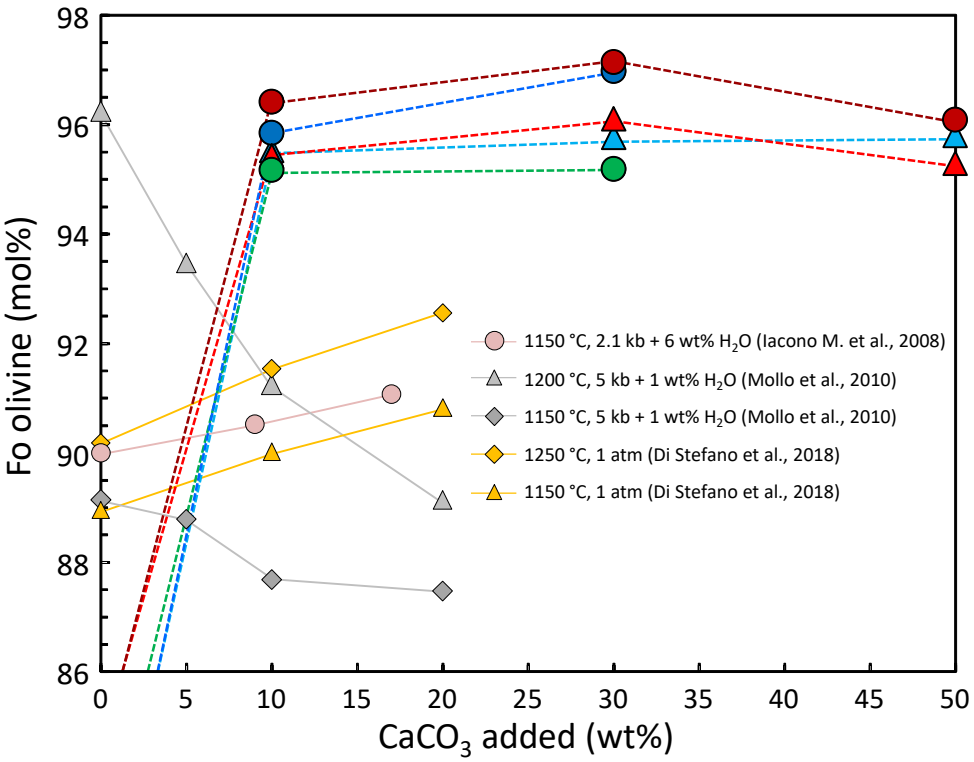
Fo olivine (mol%)
CaCO3 added (wt%)
1150 °C, 2.1 kb + 6 wt% H2O (Iacono M. et al., 2008)
1200 °C, 5 kb + 1 wt% H2O (Mollo et al., 2010)
1150 °C, 5 kb + 1 wt% H2O (Mollo et al., 2010)
1250 °C, 1 atm (Di Stefano et al., 2018)
1150 °C, 1 atm (Di Stefano et al., 2018)

Fig. 2

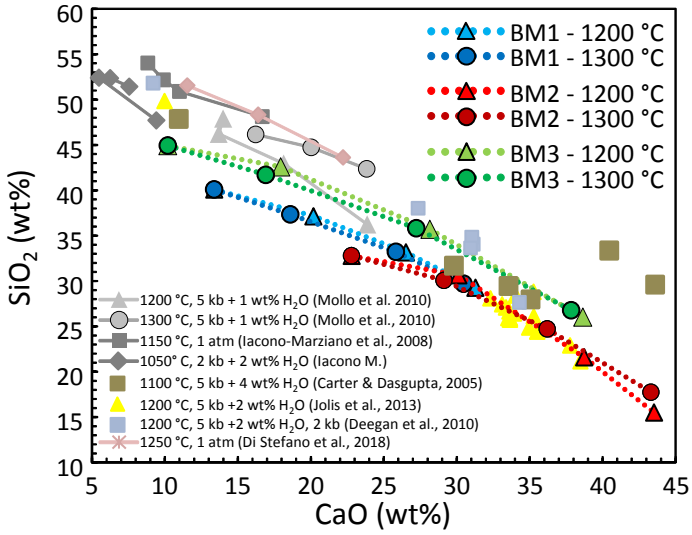

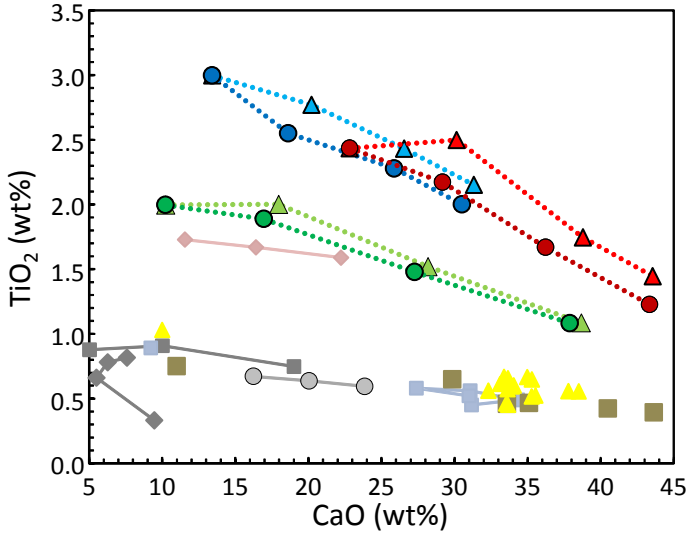

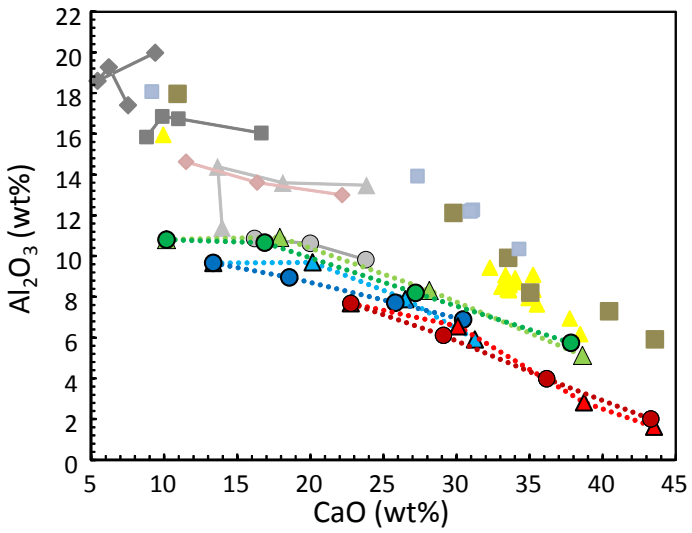

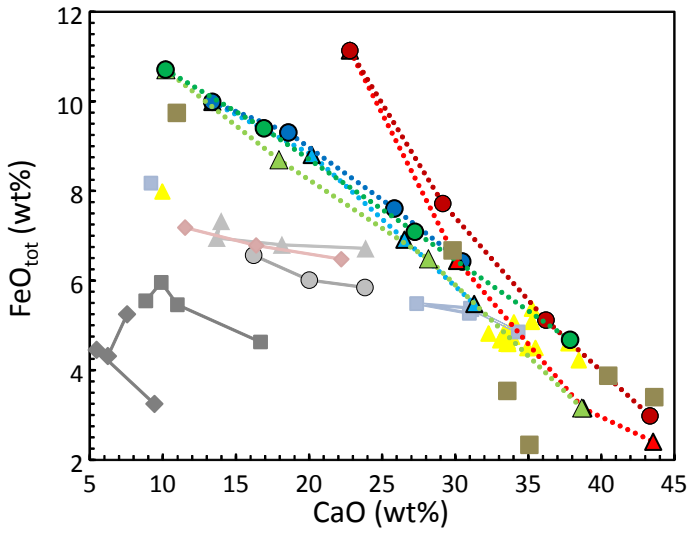

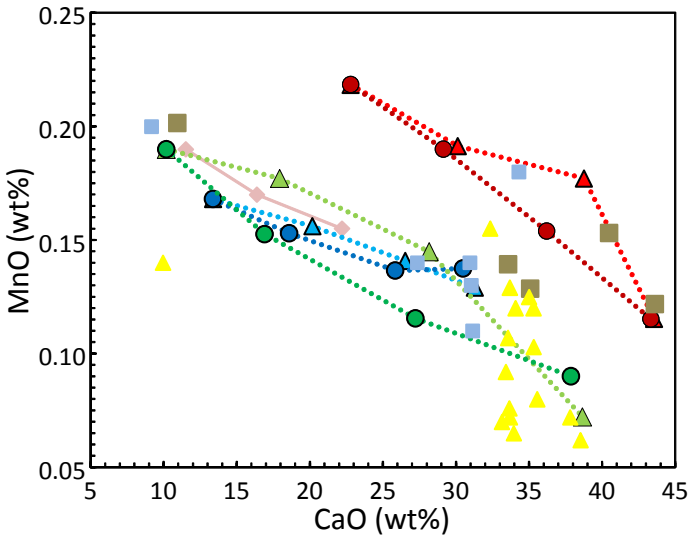

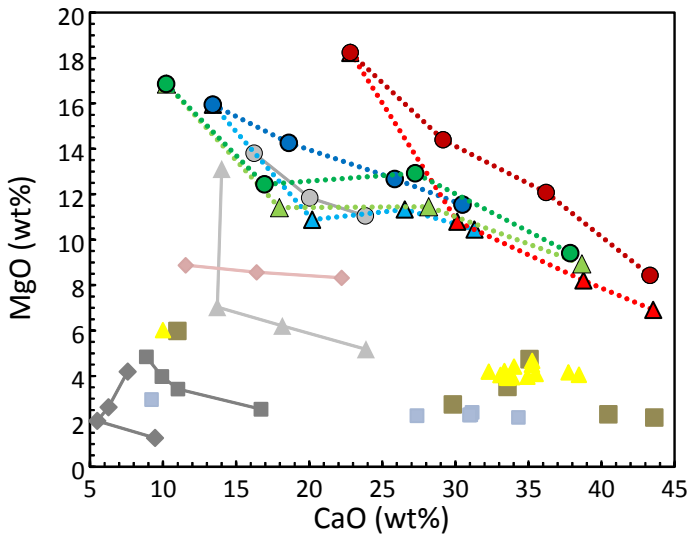

Lustrino et al. (Accepted for publication in Geology)
Supplementary Figures

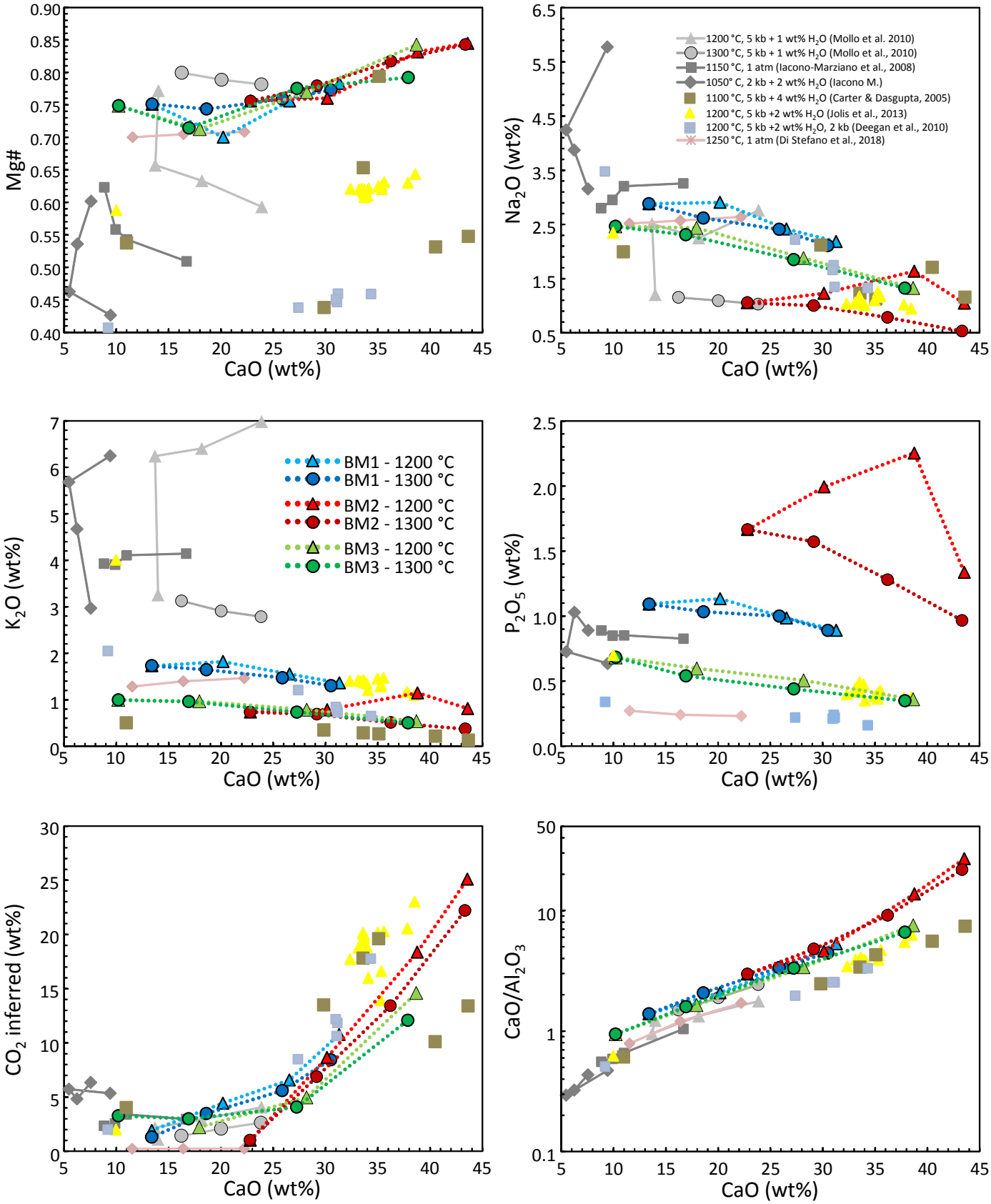

Lustrino et al. (Accepted for publication in Geology)
Supplementary Figures

Data Repository

Experimental evidence on the origin of Ca-rich carbonated melts formed by interaction between sedimentary limestones and mantle-derived ultrabasic magmas

Michele Lustrino[1,2], Natascia Luciani[1,3], Vincenzo Stagno[1,5], Silvia Narzisi[1], Matteo Masotta[4], Piergiorgio Scarlato[5]*

1 Dipartimento di Scienze della Terra, Sapienza Università di Roma, P.le A. Moro, 5, 00185 Roma, Italy
2 CNR – Istituto di Geologia Ambientale e Geoingegneria (IGAG), c/o Dipartimento di Scienze della Terra, Sapienza Università di Roma, P.le A. Moro, 5, 00185 Roma, Italy
3 Faculty of Science, Vrije Universiteit Amsterdam, De Boelelaan 1085, 1081 HV Amsterdam, the Netherlands
4 Dipartimento di Scienze della Terra, Università degli Studi di Pisa, Via S. Maria, 53, 56126, Pisa, Italy
5 Istituto Nazionale di Geofisica e Vulcanologia, Sezione di Roma1, Via di Vigna Murata, 605, 00143, Roma, Italy
* Corresponding author. email: michele.lustrino@uniroma1.it

Experimental and Analytical Procedures

The starting material used for this study was prepared starting from a Paleocene monticellite-bearing melilitite (vesecite, Vesec, Czech Republic; BM2), a Paleocene melilitite-olivine-nephelinite (polzenite, Osečná Complex, Czech Republic; BM1), and a basanite (Jauernick, Germany; BM3). The three samples were melted at 1400 °C for two hours using a vertical furnace RHTV 120-300/18 (Nabertherm) and then quenched in water. The glass was then powdered and melted again at 1450 °C for four hours in the same furnace and then reduced to powder again. The composition of the volatile-bearing natural samples and that of the volatile-free glasses are reported in Table 1. The powders were eventually mixed with different amounts (10, 30 and 50 wt%) of $CaCO_3$ (99.9% purity; AlfaAesar) to obtain three mixtures for each samples (Table 1).

In each experiment the 3 mixtures starting materials were loaded in Pt capsules with a length of ~6-9 mm and ~3 mm to ensure the same P-T conditions. Subsequently, the capsules were welded at the bottom using Welding Microscopes - Lampert PUK U3 under Ar atmosphere. The experiments were performed in a non-end loaded piston cylinder ("QUICKpress" design by Depths of the Earth Co.; Masotta et al., 2012) available at the HP-HT laboratory of the INGV in Rome (Fig. 1). This device generates high pressures (up to 10 kbar) by a hydraulic oil system that pushes a piston into a cylinder consisting of concentric layers of hardened-steel around a WC (tungsten carbide) core. The pressure is estimated from the ratio of hydraulic oil force that is necessary to drive the main ram and the area ratio between the ram and the piston. The uniaxial pressure is then distributed hydrostatically over the sample through deformation of the cell assembly materials. The high temperature is generated by applying a regulated voltage through a cylindrical graphite furnace surrounding the sample. The temperature is monitored with a C-type (W95Re5-W74Re26) thermocouple placed to one end of the capsule.

The 19-25 mm assembly (numbers referred to outer diameter of assembly; Figure 2) has been used for the experiments. It consists of a 11 mm outer diameter graphite furnace, a borosilicate glass insulator (diameter 19 mm), all hosted by an outer NaCl cylinder that fits inside the WC

bomb. The sample container used was a modified drilled MgO rod with three holes with diameter of 2 mm. In this way three Pt capsules could be loaded for each experimental run.

In each run, the assembly was first pressurized to a nominal pressure 10% higher than that desired for the experiment and held for few minutes. Pressure was then decreased to 2 kbar (target pressure), and maintained manually constant for the duration of the experiment.

All the experiments were performed at a pressure of 2 kbar at different temperatures, 1100 °C (QP_123, RM_44), 1200 °C (QP_125, RM_41, RM_43), and 1300 °C (QP_124, RM_37, RM_42) from 1 to 12 hours. The experiments were finally quenched manually by shutting down the power. The recovered samples were embedded in epoxy resin and polished without water to avoid dissolution of the carbonate fraction of the melt using the LaboPol-5 Struers using SiC abrasive papers and diamond paste with 0.25 µm for final polishing.

Qualitative and semi-quantitative analyses of the samples were collected using the scanning electron microscopy (SEM) available at the Dipartimento di Scienze della Terra Sapienza University of Rome and at INGV in Rome. The instrument exploits a bundle of focused primary electrons that hit the sample. The quantitative chemical composition of the glass and mineral phases were analysed by electron probe microanalysis (EPMA) at the CNR-IGAG laboratories (Dipartimento di Scienze della Terra, Sapienza University of Rome) using a Cameca SX50 probe and at INGV in Rome, using a Jeol-JXA8200EDS-WDS.

Cameca SX50 Electron Microprobe at the CNR-IGAG lboratory operating conditions were 15 kV accelerating voltage, 15 nA beam current and 1 µm beam diameter for olivine, pyroxene and opaque minerals, 10 µm for glass. Counting times for all elements were 20 s for the peak and 10 s for the background on each side of the peak. Used standards: Na_2O = jadeite; MgO = periclase; TiO_2 = rutile; FeO = magnetite; SiO_2 and CaO = wollastonite; Al_2O_3 = corundum; MnO = rhodonite; K_2O = orthoclase; BaO = barite; SrO = celestine; NiO = metallic Ni.

Chemical analyses collected at INGV were performed using 15 kV accelerating voltage and 7.5 nA beam current and a defocused electron beam of 2.5 µm. The following standards were used for analyses: MgO = forsterite; K_2O = orthoclase; FeO = augite; Na_2O, SiO_2 and Al_2O_3 = albite; TiO_2 = rutile; CaO and P_2O_5 = fluoroapatite; MnO = rodonite, Cr = metallic Cr; Ni = metallic Ni.

Figure 1. Quick Press apparatus. Picture from http://www.depthsoftheearth.com/instrumentation.htm.

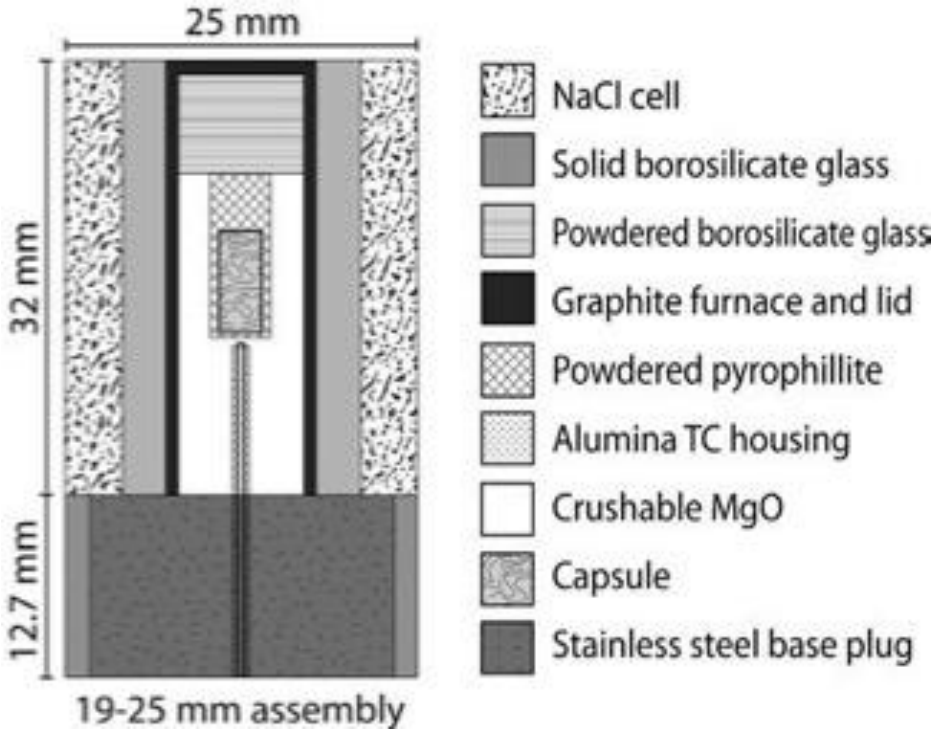

Figure 2. 19-25mm assembly for quick press used to perform the experiments (Masotta et al., 2012).

Run#	T (°C)	P (kbar)	Cc added (wt%)	SiO_2	TiO_2	Al_2O_3	FeO	MnO	MgO	CaO	Na_2O	K_2O	P_2O_5	Total	CO_2(100-tot)	CaO/Al_2O_3	Mg#
BM1 (natural sample; polzenite)				38.52	2.86	9.85	11.20	0.18	15.94	13.58	2.75	1.82	1.15	97.84	2.2	1.4	0.73
BM1 (quenched glass)			0	40.11	3.00	9.66	9.98	0.17	15.94	13.40	2.88	1.73	1.09	98.09	1.9	1.4	0.75
QP1_123_10	1100	2	10	38.87	2.54	10.94	7.57	0.18	5.88	22.93	3.90	2.66	1.25	96.73	3.3	2.10	0.59
QP1_123_30	1100	2	30	31.25	1.24	6.73	4.29	0.12	2.92	29.54	3.60	3.51	1.93	85.13	14.9	4.39	0.56
QP1_123_50	1100	2	50	29.49	1.23	3.98	2.05	0.14	4.57	40.40	3.36	2.08	0.73	88.03	12.0	10.15	0.81
QP1_125_10	1200	2	10	37.19	2.77	9.69	8.80	0.16	10.88	20.20	2.91	1.82	1.13	95.56	4.4	2.08	0.70
QP1_125_30	1200	2	30	33.21	2.43	7.89	6.91	0.14	11.33	26.56	2.42	1.55	0.98	93.42	6.6	3.37	0.76
QP1_125_50	1200	2	50	29.34	2.15	5.91	5.48	0.13	10.46	31.33	2.19	1.36	0.89	89.23	10.8	5.30	0.78
QP1_124_10	1300	2	10	37.40	2.55	8.95	9.30	0.15	14.26	18.61	2.62	1.65	1.03	96.52	3.5	2.08	0.74
QP1_124_30	1300	2	30	33.26	2.28	7.71	7.60	0.14	12.67	25.88	2.41	1.47	1.00	94.41	5.6	3.36	0.76
QP1_124_50	1300	2	50	29.78	2.00	6.88	6.42	0.14	11.54	30.52	2.11	1.30	0.89	91.57	8.4	4.43	0.77
BM2 (natural sample; vesecite)				30.29	2.27	7.39	11.25	0.20	17.10	21.96	0.93	0.74	1.46	93.59	6.4	3.0	0.74
BM2 (quenched glass)			0	32.84	2.44	7.68	11.12	0.22	18.23	22.82	1.06	0.74	1.66	98.80	1.2	2.97	0.76
RM41_10	1200	2	10	30.70	2.50	6.56	6.44	0.19	10.80	30.16	1.23	0.78	1.99	91.35	8.6	4.60	0.76
RM41_30	1200	2	30	21.69	1.75	2.83	3.15	0.18	8.21	38.80	1.64	1.15	2.25	81.64	18.4	13.73	0.83
RM41_50	1200	2	50	15.62	1.45	1.62	2.40	0.12	6.92	43.58	1.05	0.81	1.34	74.90	25.1	26.89	0.84
RM37_10	1300	2	10	30.13	2.17	6.10	7.71	0.19	14.39	29.19	1.01	0.69	1.57	93.14	6.9	4.79	0.78
RM37_30	1300	2	30	24.79	1.67	3.98	5.11	0.15	12.08	36.25	0.79	0.51	1.28	86.59	13.4	9.12	0.82
RM37_50	1300	2	50	17.83	1.23	1.99	2.97	0.12	8.42	43.37	0.53	0.37	0.96	77.81	22.2	21.76	0.84
BM3 (natural sample; basanite)				43.92	1.94	10.91	11.61	0.17	16.93	10.49	2.35	1.00	0.55	99.87	0.1	1.0	0.73
BM3 (quenched glass)			0	44.95	2.00	10.81	10.70	0.19	16.86	10.21	2.47	1.00	0.68	99.84	0.2	0.94	0.75
RM44_10	1100	2	10	44.58	2.22	10.05	7.82	0.09	11.91	20.81	1.24	0.32	0.47	99.51	0.5	2.07	0.74
RM44_30	1100	2	30	42.38	0.17	6.15	2.03	0.05	12.60	33.79	0.51	0.28	0.21	98.16	1.8	5.49	0.92
RM44_50	1100	2	50	16.51	1.52	2.19	2.24	0.12	6.01	43.47	1.85	0.94	0.73	75.57	24.4	19.85	0.84
RM43_10	1200	2	10	42.63	2.00	10.92	8.69	0.18	11.41	17.95	2.44	0.96	0.60	97.78	2.2	1.64	0.71
RM43_30	1200	2	30	35.76	1.52	8.31	6.48	0.14	11.45	28.20	1.88	0.78	0.51	95.04	5.0	3.39	0.77
RM43_50	1200	2	50	26.10	1.09	5.13	3.16	0.07	8.94	38.69	1.33	0.54	0.36	85.40	14.6	7.54	0.84
RM42_10	1300	2	10	41.74	1.89	10.65	9.39	0.15	12.44	16.94	2.31	0.96	0.54	97.01	3.0	1.59	0.71
RM42_30	1300	2	30	35.85	1.48	8.19	7.08	0.12	12.93	27.27	1.85	0.73	0.44	95.94	4.1	3.33	0.78
RM42_50	1300	2	50	26.85	1.08	5.74	4.67	0.09	9.41	37.90	1.33	0.50	0.35	87.92	12.1	6.60	0.79

Table 1. Natural samples and quenched glasses used for experiments. Mg# = 100 x Mg/(Mg+Fe^{2+}) assuming Fe^{3+}/Fe = 0.15.

T= 1100 °C BM1 QP_123

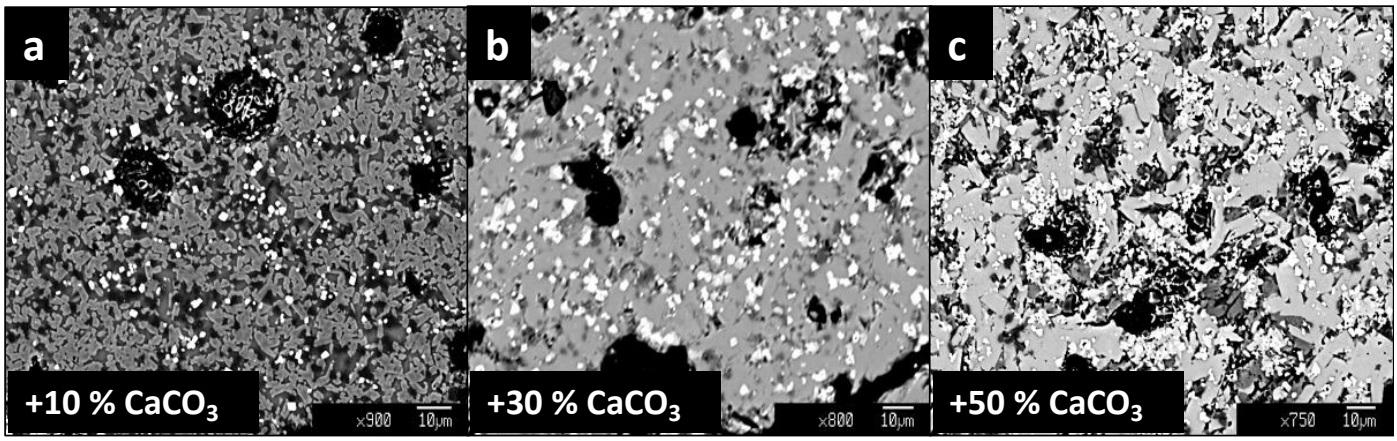

Figure 3. BSE images relative to QP123 run with BM1 starting material at 2 kbar and 1100 °C as function of the $CaCO_3$ content mixed with the starting glass used for our experiments.

T= 1100 °C BM3 RM_44

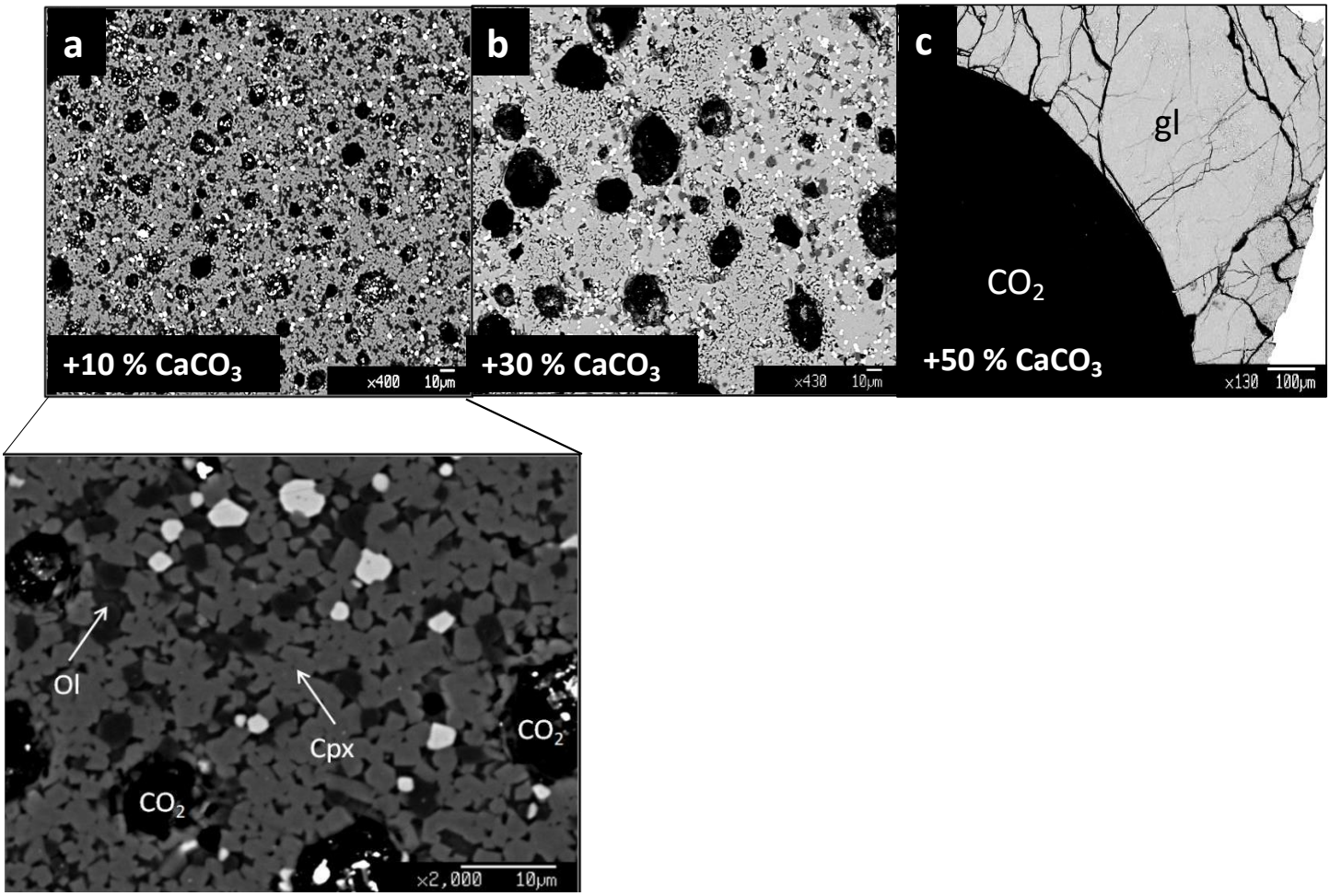

Figure 4. BSE images relative to RM44 run with BM31 starting material at 2 kbar and 1100 °C as function of the $CaCO_3$ content mixed with the starting glass used for our experiments. Ol = olivine. Cpx = clinopyroxene.

T= 1200 °C BM1 QP_125

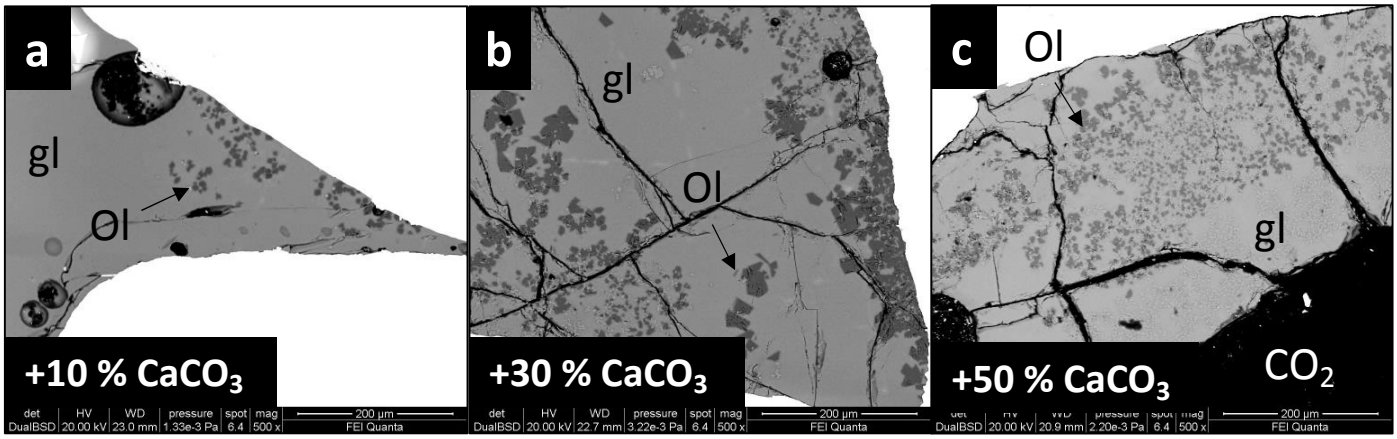

Figure 5. BSE images relative to QP1_125 run with BM1 starting material at 2 kbar and 1200 °C as function of the $CaCO_3$ content mixed with the starting glass used for our experiments. Ol = Olivine. Gl = Glass.

T= 1200 °C BM2 RM_41

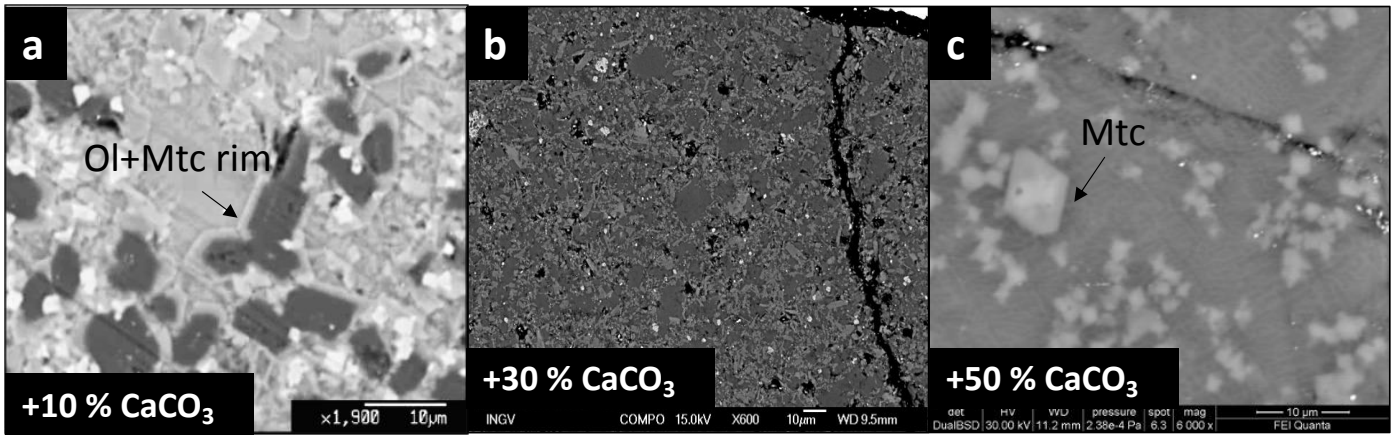

Figure 6. BSE images relative to RM_41 run with BM1 starting material at 2 kbar and 1200 °C as function of the $CaCO_3$ content mixed with the starting glass used for our experiments. Ol = olivine; Mtc = monticellite.

T= 1200 °C BM3 RM_43

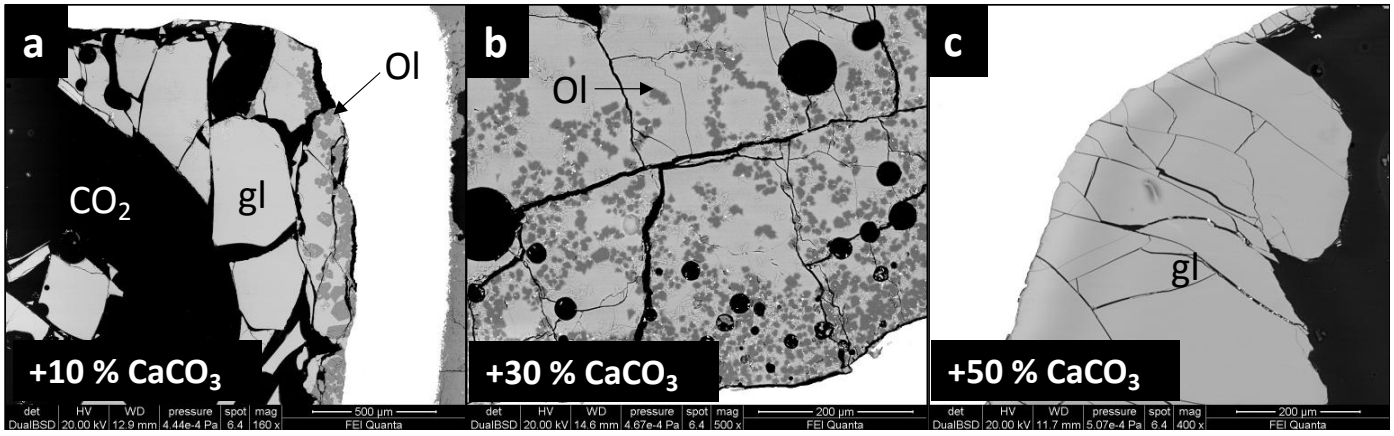

Figure 7. BSE images relative to RM_43 run with BM3 starting material at 2 kbar and 1200 °C as function of the $CaCO_3$ content mixed with the starting glass used for our experiments. Ol = olivine; Gl = Glass

T= 1300 °C BM1 QP_124

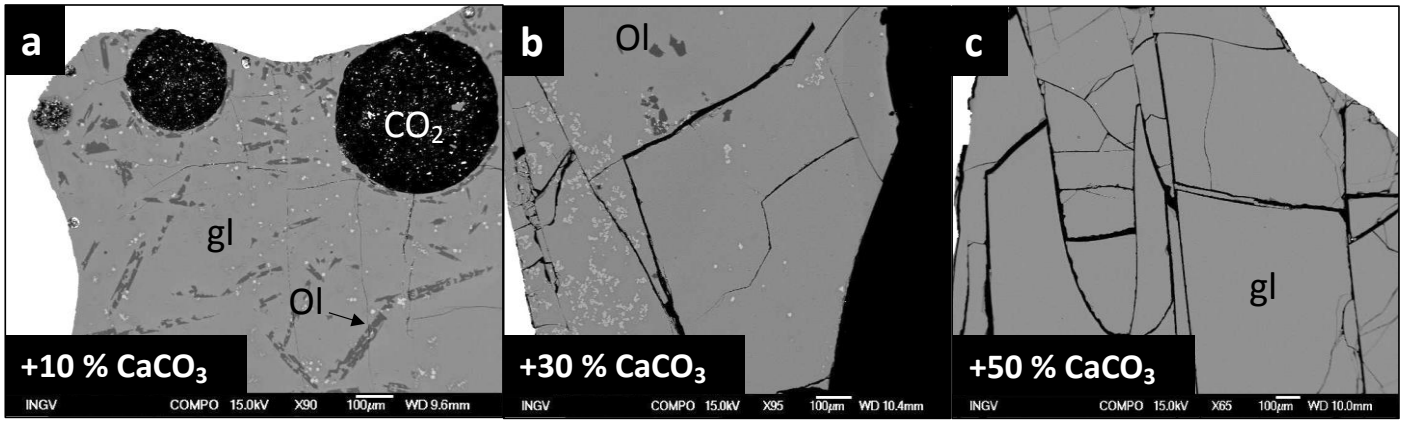

Figure 8. BSE images relative to QP_124 run with BM1 starting material at 2 kbar and 1300 °C as function of the $CaCO_3$ content mixed with the starting glass used for our experiments. Ol = olivine; Gl = Glass.

T= 1300 °C BM2 RM_37

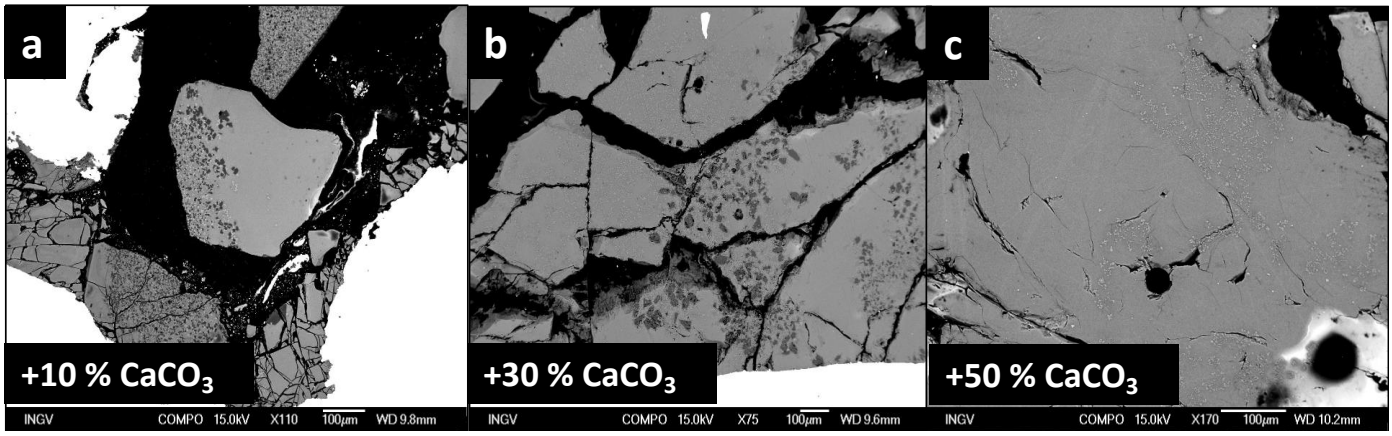

Figure 9. BSE images relative to RM_37 run with BM2 starting material at 2 kbar and 1300 °C as function of the $CaCO_3$ content mixed with the starting glass used for our experiments.

T= 1300 °C BM3 RM_42

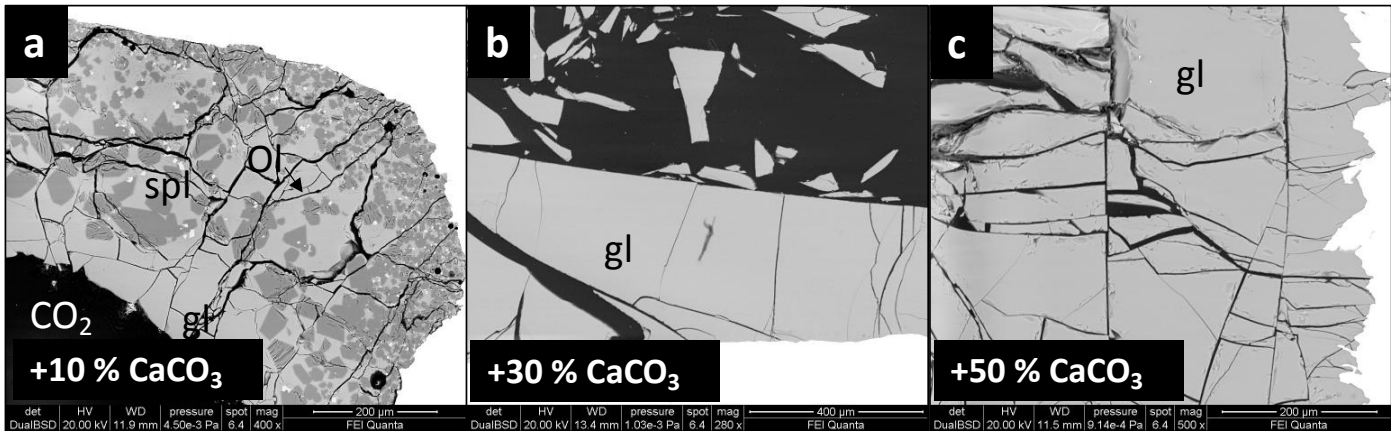

Figure 10. BSE images relative to RM_42 run with BM3 starting material at 2 kbar and 1300 °C as function of the $CaCO_3$ content mixed with the starting glass used for our experiments. Spl = Spinel. Ol = olivine. Gl = glass.

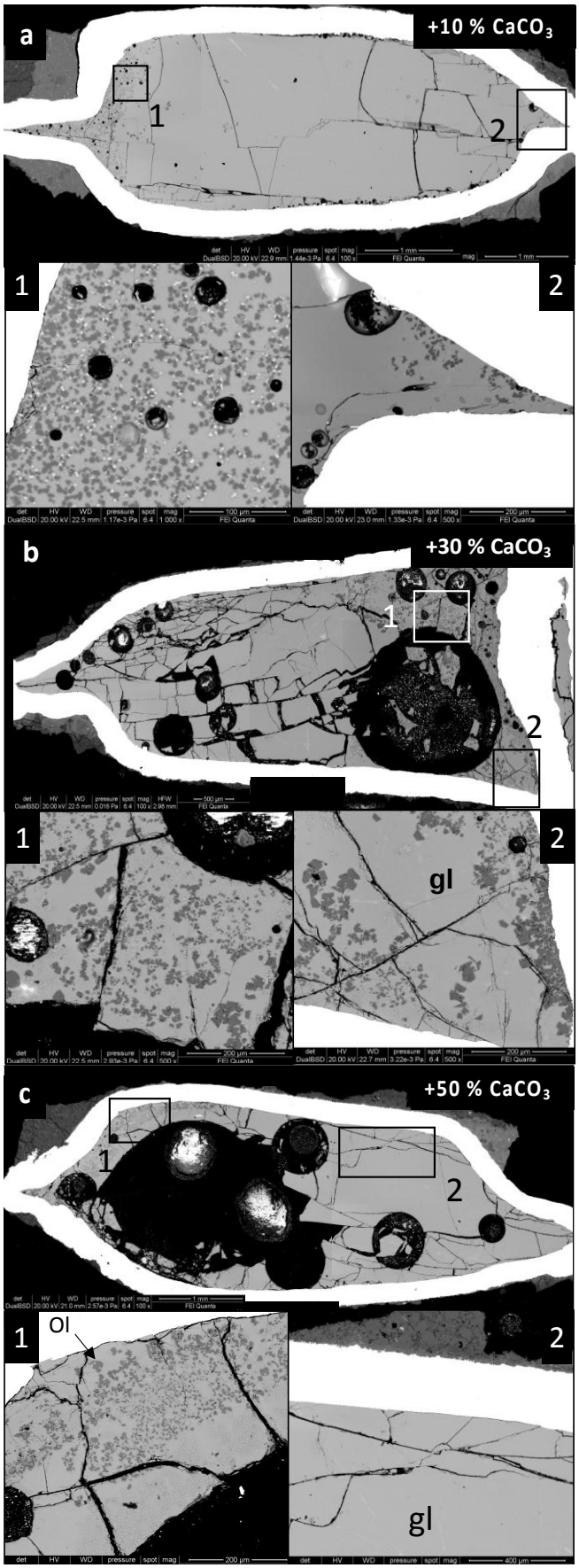

Figure 11. BSE images relative to the details of QP1_125 run with BM1 starting material at 2 kbar and 1200 °C as function of the $CaCO_3$ content mixed with the starting glass used for our experiments. Ol = Olivine. Gl = Glass.

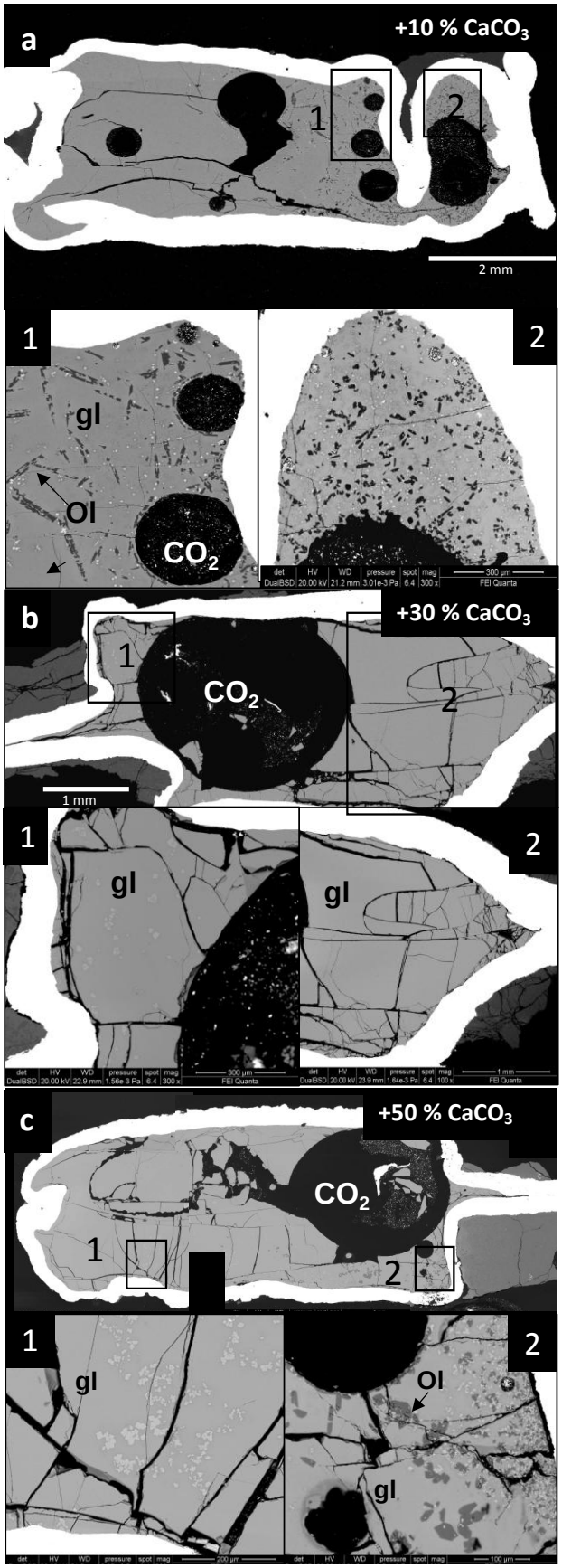

Figure 12. BSE images relative to the details of QP1_124 run with BM1 starting material at 2 kbar and 1300 °C as function of the $CaCO_3$ content mixed with the starting glass used for our experiments. Ol = Olivine. Gl = Glass.

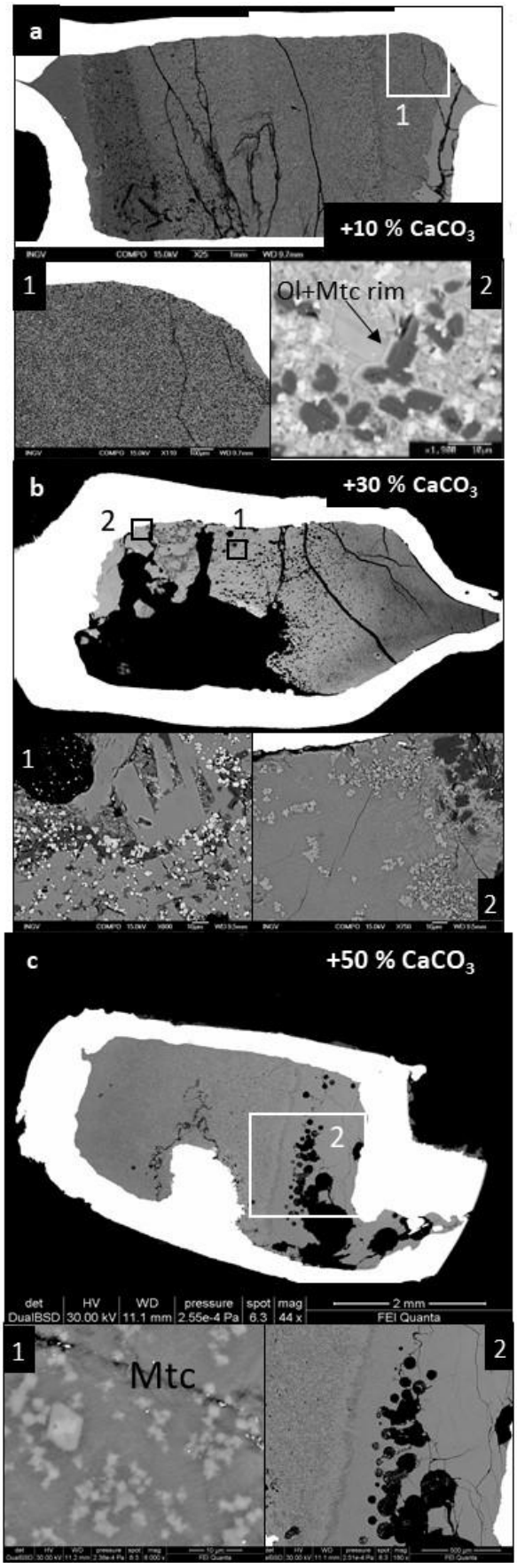

Figure 13. BSE images relative to the details of RM41 run with BM2 starting material at 2 kbar and 1200 °C as function of the $CaCO_3$ content mixed with the starting glass used for our experiments. Ol = Olivine. Mtc = monticellite.

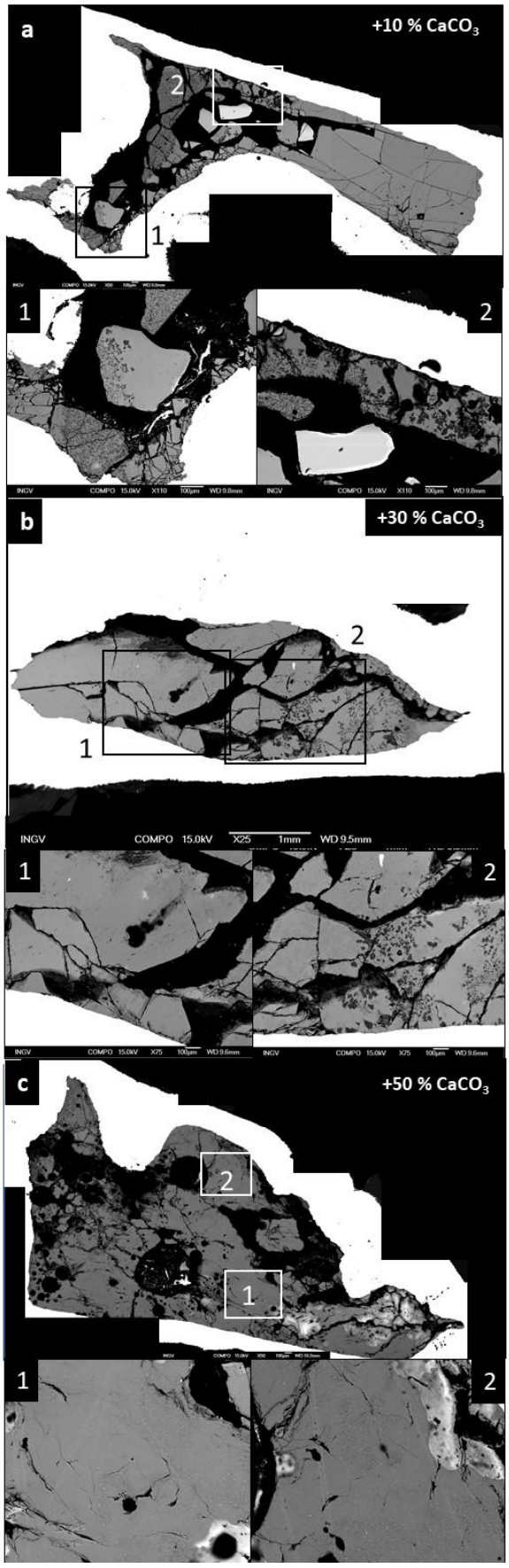

Figure 14. BSE images relative to the details of RM37 run with BM2 starting material at 2 kbar and 1300 °C as function of the $CaCO_3$ content mixed with the starting glass used for our experiments.

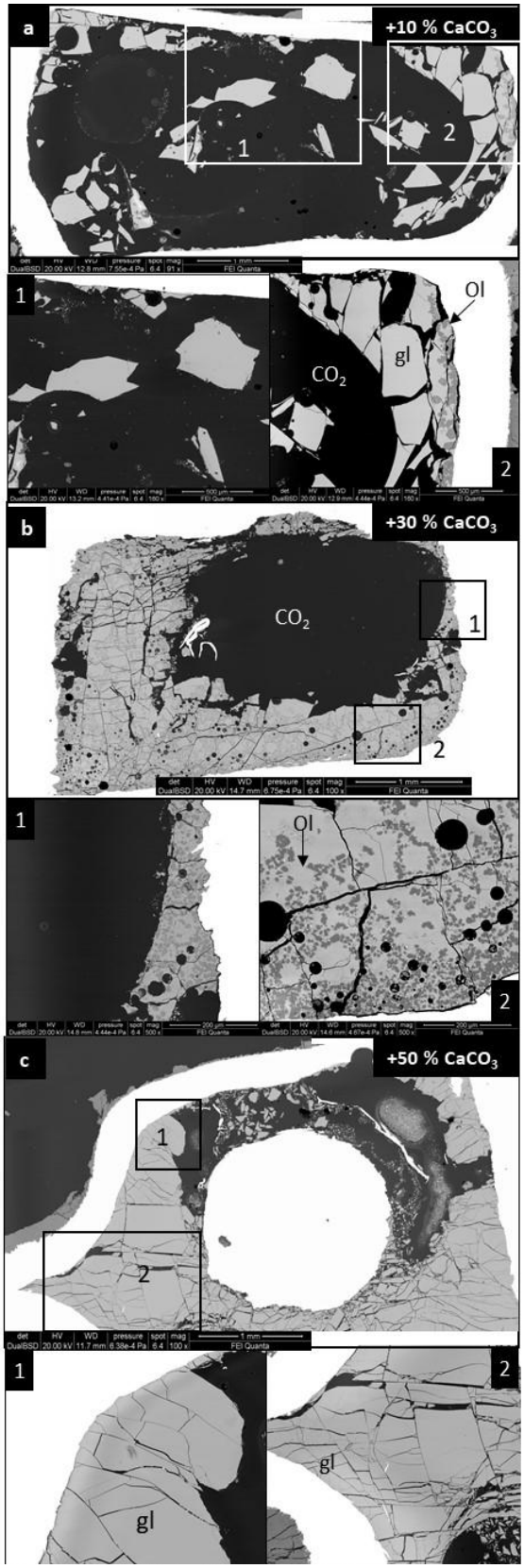

Figure 15. BSE images relative to the details of RM43 run with BM3 starting material at 2 kbar and 1200 °C as function of the $CaCO_3$ content mixed with the starting glass used for our experiments. Ol = olivine; Gl = glass.

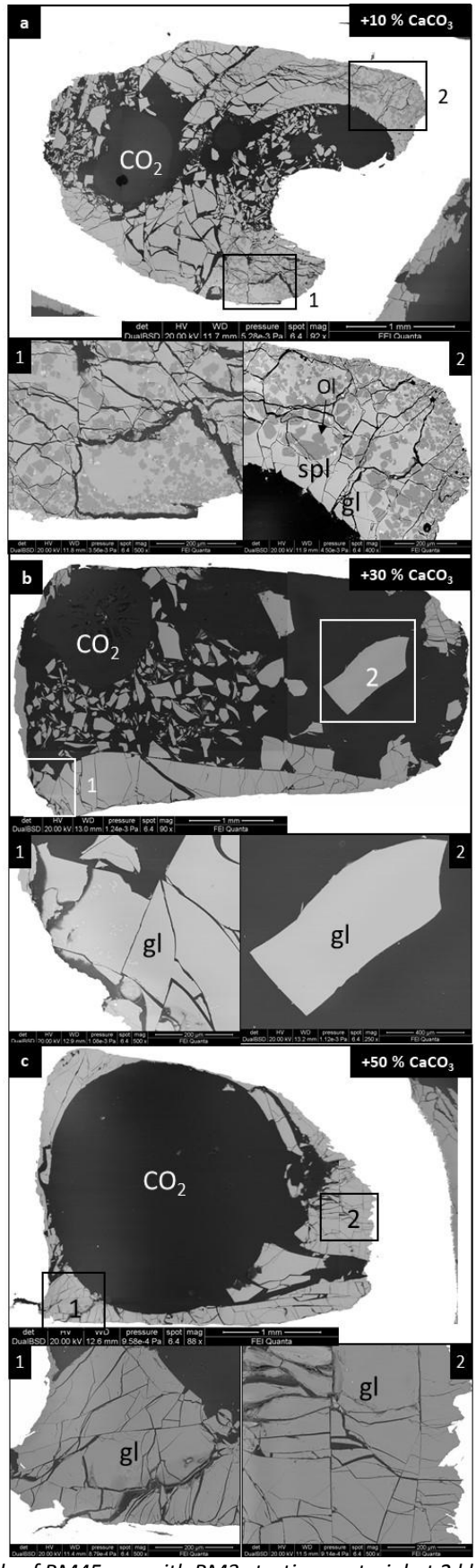

Figure 16. BSE images relative to the details of RM45 run with BM3 starting material at 2 kbar and 1300 °C as function of the $CaCO_3$ content mixed with the starting glass used for our experiments. Ol = olivine;Spl = spinel; Gl = glass.